New Journal of Physics
The open access journal at the forefront of physics

Deutsche Physikalische Gesellschaft DPG
IOP Institute of Physics

Published in partnership with: Deutsche Physikalische Gesellschaft and the Institute of Physics

OPEN ACCESS

RECEIVED
17 August 2016

REVISED
26 October 2016

ACCEPTED FOR PUBLICATION
28 October 2016

PUBLISHED
17 November 2016

PAPER

Four-dimensional positron age-momentum correlation

Ulrich Ackermann[1,3], **Benjamin Löwe**[1,3], **Marcel Dickmann**[1,2], **Johannes Mitteneder**[1], **Peter Sperr**[1], **Werner Egger**[1], **Markus Reiner**[2] **and Günther Dollinger**[1]

[1] Universität der Bundeswehr München, Institut für Angewandte Physik und Messtechnik (LRT 2), Werner-Heisenberg-Weg 39, D-85577 Neubiberg, Germany
[2] Heinz Maier-Leibnitz Zentrum (MLZ), Technische Universität München, Lichtenbergstr. 1, D-85748 Garching, Germany
[3] These authors contributed equally to this project and should be considered co-first authors.

E-mail: benjamin.loewe@unibw.de

Keywords: 4D-AMOC, positron annihilation, CDBS, 2D-ACAR, PALS, AMOC

Abstract

We have performed first four-dimensional age-momentum correlation (4D-AMOC) measurements at a pulsed high intensity positron micro beam and determined the absolute value of the three-dimensional momentum of the electrons annihilating with the positrons in coincidence with the positron age in the sample material. We operated two position sensitive detectors in coincidence to measure the annihilation radiation: a pixelated HPGe-detector and a microchannel plate image intensifier with a $CeBr_3$ scintillator pixel array. The transversal momentum resolution of the 4D-AMOC setup was measured to be about $17 \times 10^{-3}\, m_0 c$ (FWHM) and was circa 3.5 times larger than the longitudinal momentum resolution. The total time resolution was 540 ps (FWHM). We measured two samples: a gold foil and a carbon tape at a positron implantation energy of 2 keV. For each sample discrete electron momentum states and their respective positron lifetimes were extracted.

1. Introduction

Due to their positive charge, positrons are repelled from the atomic nuclei and attractively trapped in open volume defects when implanted in matter. Therefore positrons are a powerful tool to investigate defects in solids such as vacancies, voids and dislocations [1]. Since many decades commonly used positron techniques are positron annihilation lifetime spectroscopy (PALS) [2], two-dimensional angular correlation of annihilation radiation (2D-ACAR) measurements [3], coincidence Doppler broadening spectroscopy (CDBS) [4, 5] and age-momentum correlation (AMOC) measurements [6].

When performing PALS with a pulsed positron beam, the time between the implantation of the positron in the solid and its annihilation is measured and thus an exponentially shaped positron lifetime spectrum is recorded. The positron lifetime in the open volume defects is enhanced compared to the bulk material and is thus a measure for the electron density at the annihilation site. By extracting the different positron lifetime components one can deduce type and concentration of various defects in materials.

To obtain information about the electron momentum distributions in solids CDBS and 2D-ACAR are utilised. In CDBS the longitudinal momentum of the electron annihilating with the positron is derived by measuring the energy of both annihilation gamma quanta. CDBS however is limited due to the energy resolution of the detector of about 1 keV at 511 keV [5, 7]. To measure the momenta of the valence electrons more precisely, the 2D-ACAR method is used. In 2D-ACAR the angular deviation of the 180° collinearity of the two annihilation gamma quanta is measured by a coincidence detector setup to derive the transversal momenta of the electrons. The positron lifetime and the energy of one of the annihilation quanta is measured in coincidence to perform (2D-)AMOC. It enables the simultaneous detection of the longitudinal electron momenta and the defect types with its respective concentrations. A detailed description of the above mentioned techniques can be found in [8–10].

To measure the full three-dimensional momentum of the electron in coincidence with the positron age a position sensitive fast scintillation detector and a position sensitive HPGe-detector is needed. This measurement

technique is called four-dimensional AMOC (4D-AMOC). With 4D-AMOC it is possible to detect the defect type and the chemical vicinity of the annihilation site. In comparison to 2D-AMOC one expects a higher sensitivity to distinguish the element specific electronic structures. Thus defects should be better characterised with 4D-AMOC in comparison to 2D-AMOC.

In this work we present first-time 4D-AMOC measurements investigating two different samples to demonstrate the feasibility of this new technique. Furthermore we discuss which improvements have to be made to establish 4D-AMOC as a conventional positron annihilation method in the future.

2. Experimental setup and specifications

We performed our measurements at the scanning positron microscope (SPM) interface [11–13] at the positron source NEPOMUC [14, 15] at the Munich research reactor FRM II. A pixelated HPGe-detector [16] and a position sensitive scintillation detector with a $CeBr_3$ scintillator pixel array [17] was set up at the newly installed sample chamber of the SPM interface [11]. We have investigated two samples at the SPM interface: a gold foil and a carbon tape. A VMEbus-based data acquisition system was used [16] to aquire the various signals in coincidence.

2.1. Pulsed positron beam at the SPM interface

The SPM interface has been set up to adapt the SPM at NEPOMUC [12, 13]. It produces a pulsed, sub-mm, mono-energetic positron beam after re-moderating the DC-beam created by NEPOMUC.

At the SPM interface the NEPOMUC DC-beam, which was set to an energy of 20 eV, is squeezed into bunches by a sawtooth pre-buncher and a sine wave buncher. After this, the positrons are accelerated to an energy of 5 keV and focussed onto a tungsten re-moderator which operates in reflection geometry. The re-emitted positrons are then once again bunched and the remaining continuous background is blanked out by means of a chopper. The whole pulsing system is operated at a frequency of 50 MHz which results in a time window of 20 ns. At the exit of the SPM interface the beam enters a sample chamber where it is focused magnetically onto the specimen [11]. We have characterised the beam size and the pulse width at the sample at a beam energy of 2 keV, which was also the energy used during the measurements. A beam diameter of 200 μm (FWHM) and a pulse width of 320 ps (FWHM) was obtained. A higher implantation energy would have been favourable to avoid positron diffusion back to the surface and annihilation in surface states. Unfortunately this was not possible as it would have increased the size of the beam spot significantly.

2.2. Detectors

2.2.1. Scintillation detector

We used a Photek IPD340/Q/BI/RS microchannel plate image intensifier (MCPII) with an active diameter of 40 mm. The MCPII exhibits a microchannel plate (MCP) stack in chevron configuration (10 μm pores, thickness to pore diameter ratio 50:1 and 80:1 for the upper and lower MCP) and a bialkali photocathode evaporated onto the 9 mm thick fused silica entrance window.

By using the high viscosity coupling grease Rhodorsil 47 V 100 000 a Scionix $CeBr_3$ scintillator pixel array (pixel dimension 2.5 mm × 2.5 mm × 8 mm; each pixel wrapped with polytetrafluoroethylene (PTFE) tape; pixel pitch 3.3 mm) was coupled to the entrance window and covered the whole active area of the MCPII. The $CeBr_3$ pixels were, due to their high hygroscopicity, hermetically sealed in a metal case with a 1.5 mm thick fused silica window. In this work a total of 104 pixels were utilised for the determination of the position.

The electron cloud produced in the channels of the MCP stack of the MCPII is collected on a resistive anode. To derive the two dimensional position, a 2D-backgammon anode is capacitively coupled from the outside of the MCPII to the resistive anode. At a gamma energy of 511 keV (^{22}Na) the position resolution of the scintillation detector is limited by the pixel cross section. The best single time resolution at a gamma energy of 511 keV (^{22}Na) was about 320 ps (FWHM) located around the centre of the MCPII. The single time resolution is about a factor 2 to 3 worse at the edge of the active area of the MCPII. A detailed description of the scintillation detector can be found in [17].

2.2.2. Pixelated high purity germanium detector

The position sensitive HPGe-detector (Canberra EGPS 48*48*20-36 PIX) consists of a planar germanium crystal with a thickness of 20 mm segmented into 6 × 6 pixel contacts (8 mm × 8 mm each). A gamma ray which hits a pixel induces a charge in the neighbour pixels. Thus, by taking also these induced charges into account, the position sensitivity is smaller than the pixel size. At a gamma energy of 662 keV (^{137}Cs) an energy resolution of 1.33 keV and a position resolution of 1.6 mm has been achieved [16].

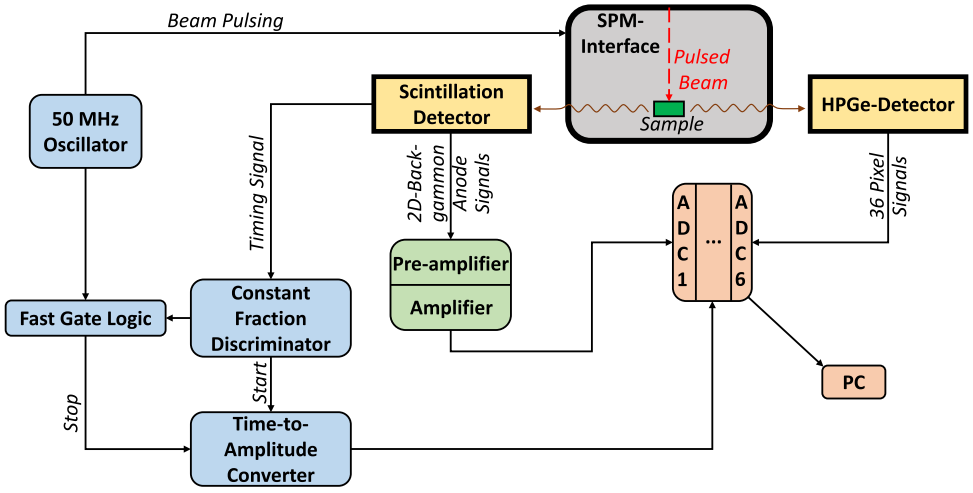

Figure 1. Scheme of the 4D-AMOC detector setup and the signal acquisition. See [18, 19] for a detailed description of the timing electronics (blue).

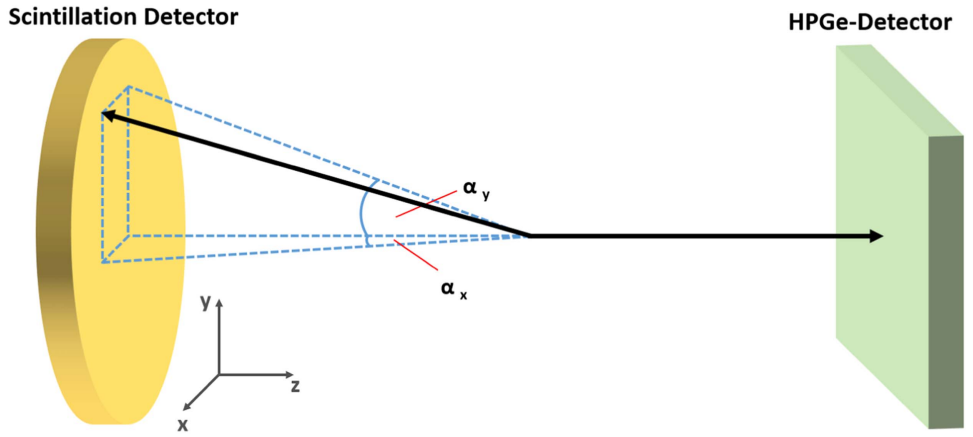

Figure 2. Scheme of the detector arrangement and the angular deviations α_x and α_y. The two black arrows indicate the annihilation radiation produced at the sample.

2.2.3. Detector arrangement

A schematic diagramm of our detector arrangement can be seen in figures 1 and 2. The two detectors were in a 180° arrangement to measure both annihilation quanta in coincidence. The detector distance to the sample was 21 cm for the scintillation detector and 15.5 cm for the pixelated HPGe-detector in order to have comparable angular resolutions.

2.3. Data acquisition and analysis

We adapted a data acquisition and analysis system which was already used in an earlier version for the position resolution measurements of the HPGe-detector [16]. The data acquisition is based on a VME-system and the data analysis on the ROOT framework [20, 21] and the Qt application framework [22]. We used the HistPresent program [23] from the MARaBOU data acquisition system [24, 25] for online histogram visualisation. Six Struck SIS3302 eight-channel analog-to-digital converters were utilised to process the 36 pre-amplifier pixel outputs of the HPGe-detector, the four amplifier outputs of the scintillation detector and the TAC signal. In figure 1 a schematic of the detector signal acquisition is given.

For the scintillation detector as well as for the pixelated HPGe-detector an energy window was set on the 511 keV photopeak. Furthermore the data analysis software only processed events for which the deposited energy in the HPGe-detector was higher than 511 keV. This reduces the number of small-angle scattered photons which would increase the background events of our measurements.

2.3.1. Positron lifetime measurements

To measure the positron lifetime we fed the timing signal of the scintillation detector into a constant fraction discriminator (CFD) to generate the start signal for the time-to-amplitude converter (TAC). The stop signal was produced by a fast gate logic (FGL) utilising the 50 MHz oscillator from the beam pulsing and the CFD signal [18]. From the measured time differences between the start and stop signals we obtained the positron lifetime spectrum $L(t)$ which can be expressed by:

$$L(t) = \left[\sum_{i=1}^{N} \frac{I_i}{\tau_i} \exp(-t/\tau_i)\right] * W(t) + \mathrm{BG}, \tag{1}$$

where τ_i is the ith positron lifetime and I_i is the ith intensity. $W(t)$ is defined as the instrument resolution function and BG is the background that we assume is mainly caused by the chopper of our pulsing unit which does not completely blank out the remaining DC part of the beam. Background events due to backscattered positrons that annihilate elsewhere in the sample chamber are mostly suppressed by our coincident detector set-up. The term $\exp(-t/\tau_i)$ is implicitly assumed to be 0 for $t < 0$.

2.3.2. Three-dimensional electron momentum measurements

To deduce the three-dimensional momentum of the electron annihilating with the positron the angular correlation of the annihilation radiation was measured with both detectors and the Doppler broadening of one of the annihilation gamma quanta was acquired with the pixelated HPGe-detector.

The angular correlation of the two gamma quanta was derived by the two-dimensional position of interaction of the gamma quanta for both detectors as described in section 2.2. Angular deviations from the 180° angular correlation in x- and y-direction (α_x, α_y) can be deduced by the measured positions. Therefore the electron momenta in x- and y-direction are given by [1]:

$$p_x = \alpha_x \, m_0 c, \tag{2a}$$

$$p_y = \alpha_y \, m_0 c. \tag{2b}$$

The angular deviations α_x and α_y are depicted in figure 2. A measured angular deviation of 1 mrad is equivalent to a momentum of $10^{-3}\ m_0 c$.

By measuring the Doppler broadening ΔE of the 511 keV photopeak with the HPGe-detector one receives the electron momentum in z-direction (longitudinal electron momentum p_l) [1]:

$$p_z = p_\mathrm{l} = \frac{2\Delta E}{c}. \tag{3}$$

The absolute value of the three-dimensional momentum $|\vec{p}\,|$ of the electron is given by:

$$|\vec{p}| = \sqrt{p_x^2 + p_y^2 + p_z^2} = \sqrt{p_\mathrm{t}^2 + p_\mathrm{l}^2}, \tag{4}$$

where the transversal electron momentum p_t is defined as:

$$p_\mathrm{t} = \sqrt{p_x^2 + p_y^2}. \tag{5}$$

2.4. Samples

We investigated two samples: a gold foil and a double sided adhesive carbon tape. The gold foil had a thickness of 10 μm and a purity of 99.999%. The carbon tape has been purchased from Electron Microscopy Sciences (product code 77817-12) and had a thickness of about 0.16 mm [26].

The samples were tilted by an angle of about 45° relative to the incoming beam to minimise the shielding of the annihilation radiation in the direction to the detectors by the sample holder. The wall thickness of the sample chamber was reduced to 1.5 mm between the sample and each detector.

3. Measurements of the positron lifetime at PLEPS

We characterised the samples with PALS measurements at the pulsed low energy positron system (PLEPS) [27, 28] prior to the 4D-AMOC measurements at the SPM interface (section 4). This was done to be able to verify our lifetime spectra obtained by the 4D-AMOC measurements and to derive the lifetimes and intensities necessary for the analysis of the 4D-AMOC data (section 4.3.4). PLEPS is also located at NEPOMUC. The positron implantation energy at the sample was 2 keV and each positron lifetime spectrum contained 4×10^6 counts. The total time resolution of PLEPS was about 280 ps (FWHM).

Three positron lifetimes and their respective intensities in percent could be extracted for the gold foil PALS measurements: $\tau_1 = 175$ ps (22.4%), $\tau_2 = 347$ ps (77.3%) and $\tau_3 = 2454$ ps (0.3%). τ_1 and τ_2 can be explained

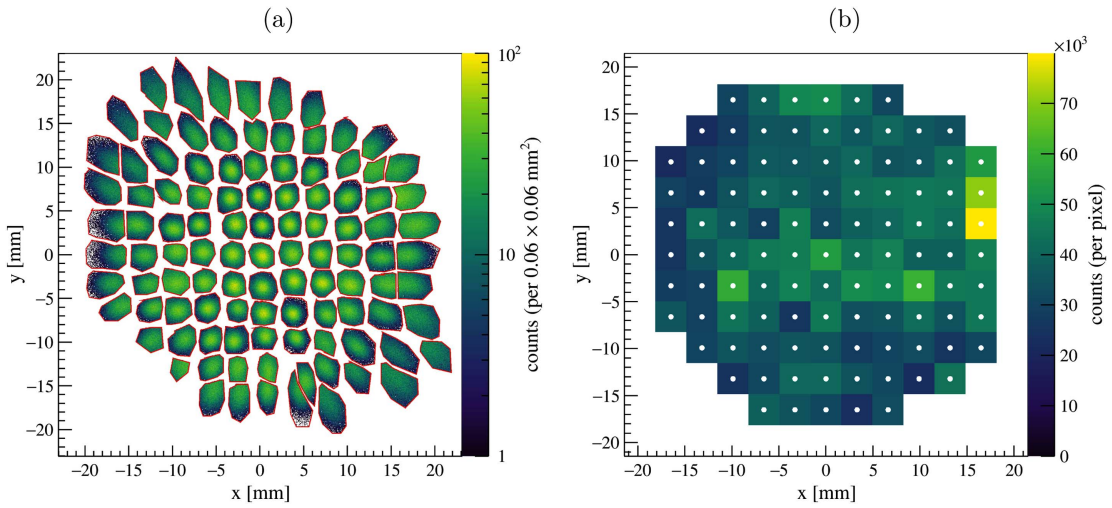

Figure 3. Non-coincident position spectra of the scintillation detector recorded during the measurement with the gold foil. (a) An energy window was set for each scintillator pixel on the 511 keV photopeak. Via cuts (red line) only events close to the scintillator pixel centre were selected to suppress Compton-scattered gamma quanta. (b) Discretized position spectrum of the scintillation detector. The events in the respective cuts of figure 3(a) were assigned to the physical centre of the appropriate scintillator pixel (indicated as white points). Thus the discretized position spectrum consists of infinitesimal small points which are at the physical centre of the scintillator pixel (for better visibility the whole areas around the white points have been coloured).

due to positron annihilation in vacancies [29, 30] and in surface states [31], respectively. τ_3 is most probably due to contaminants on the surface.

The four extracted positron lifetimes and their respective intensities of the carbon tape were: $\tau_1 = 162$ ps (13.9%), $\tau_2 = 380$ ps (52.2%), $\tau_3 = 1029$ ps (5.9%) and $\tau_4 = 3013$ ps (28.0%). τ_1 can be assigned to intrinsic para-positronium annihilation. τ_2 is due to annihilations of positrons which do not form positronium, i.e. free positrons. τ_3 and τ_4 can be assigned to the annihilation from ortho-positronium pick off annihilation [32, 33]. Another possible explanation for τ_3 might be a bound state of the positron at the interface between the carbon particles and the polymer (adhesive). In the rest of this work we assume ortho-positronium annihilation for τ_3.

4. 4D-AMOC measurements: results and discussion

4.1. Momentum sampling function

The momentum sampling function (MSF) gives the probability that a certain angular deviation of two annihilation quanta can be measured with the utilised coincident detector setup. It is influenced by the position dependent detection probability of each detector and its arrangement with respect to the other. The MSF can be determined through the convolution of the non-coincident position spectra of the two detectors [34]. During the 4D-AMOC measurements the non-coincident events of each detector were recorded together with the coincident events. Therefore no separate measurement was necessary to determine the MSF.

Figures 3 and 4 show the non-coincident position spectra with an energy window set on the 511 keV photopeak recorded during the measurement with the gold foil. As the position resolution is limited by the cross section of the $CeBr_3$ scintillator pixels we have set cuts around the events of each pixel (figure 3(a)) and assigned each cut to one discrete position defined by the physical centre of the corresponding scintillator pixel (figure 3(b)). In figure 3(b) the discretized position spectrum can be seen. The random like variations of the number of events per pixel mainly arise due to the set cuts (figure 3(a)) and energy windows.

In figure 4 the non-coincident position spectrum of the HPGe-detector is shown. The energy window was set on the 511 keV photopeak. Variations in the number of events arise mainly from charge sharing between the pixels which decreases the detection probability.

Figure 5 shows the MSF of the measurement with the gold foil that has been calculated from the non-coincident position spectra from figures 3(b) and 4. From the measurement on the carbon tape a separate MSF has been determined. The angle resolved measurements presented in this work have all been corrected by the corresponding reciprocal value of the MSF. Events with a relative detection efficiency below a threshold of 0.1 were disregarded and therefore do not appear in the spectra.

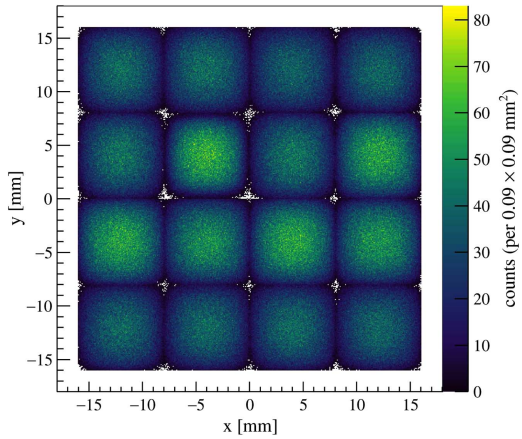

Figure 4. Non-coincident position spectrum of the pixelated HPGe-detector recorded during the measurement with the gold foil. An energy window was set on the 511 keV photopeak.

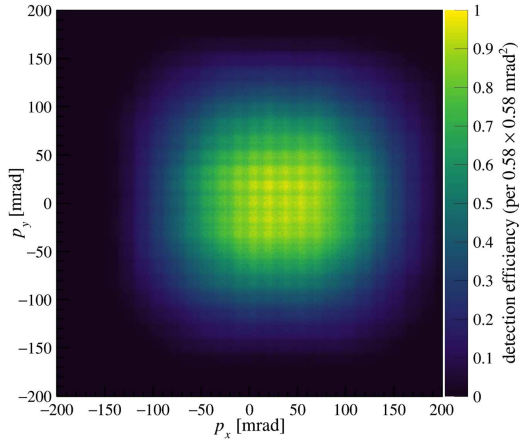

Figure 5. The momentum sampling function of the measurement with the gold foil: it was determined by convolving the two detector non-coincident position spectra from figures 3(b) and 4 (converted to mrad relative to the sample position).

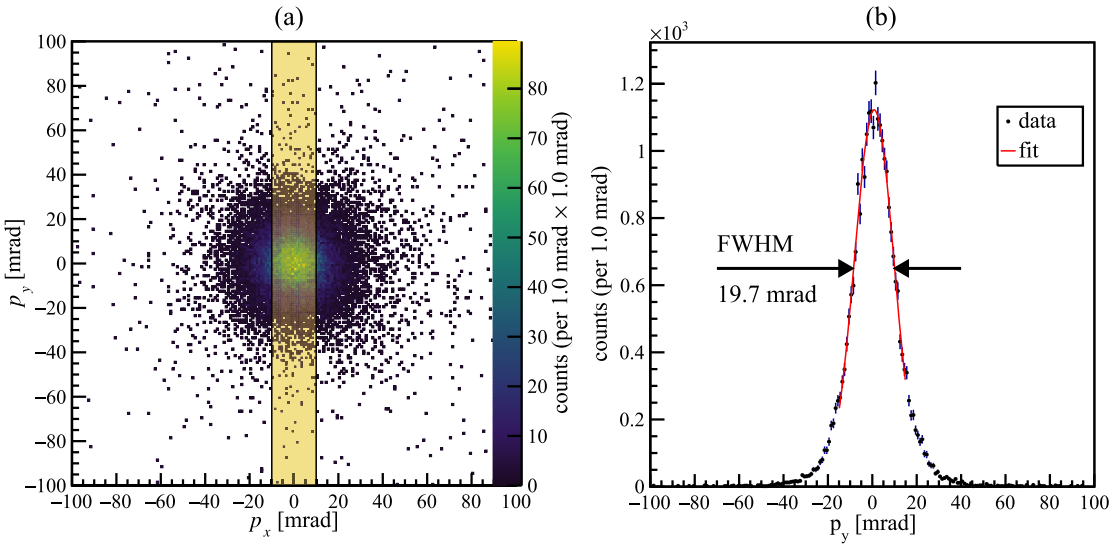

Figure 6. (a) 2D-ACAR spectrum of the gold foil. (b) Projection of the events inside the box of figure 6(a) onto the *y*-axis. A width of about 20 mrad (FWHM) was determined by fitting a Gaussian to the distribution.

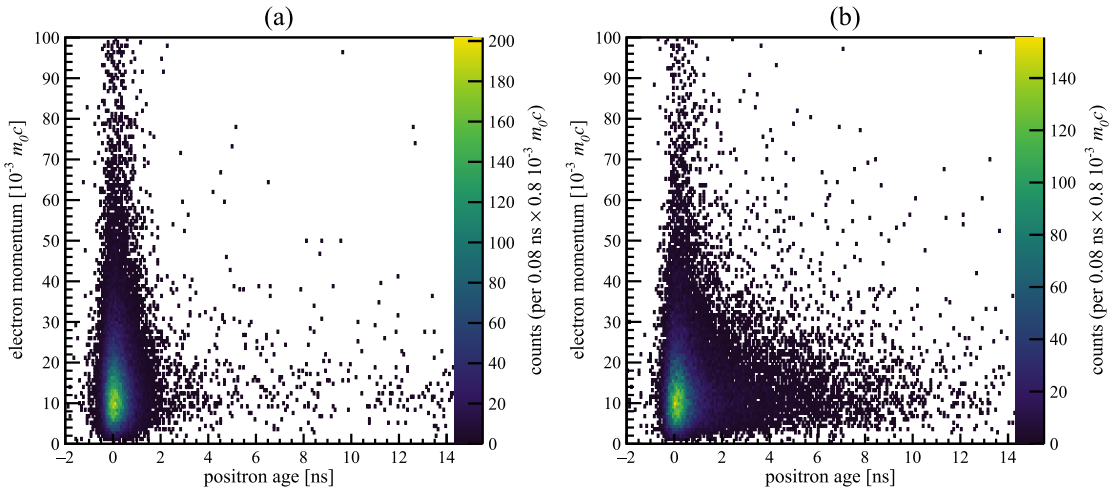

Figure 7. 4D-AMOC spectra of (a) the gold foil and (b) the carbon tape.

4.2. Determination of the angular resolution

In the 2D-ACAR spectrum of the gold foil (figure 6(a)) the transversal momenta (p_x, p_y) of the electrons annihilating with the positrons are shown. To determine the angular resolution in y-direction of our 4D-AMOC setup we projected the events of the 2D-ACAR spectrum onto the y-axis. Only events from $p_x = -10$ mrad to $+10$ mrad were taken into account. The width of the distribution was determined to be 20 mrad (FWHM). This width is defined by the angular resolution and the contribution of the transversal electron momenta. By taking the contribution of the transversal electron momenta into account one can deduce an angular resolution of about 17 mrad. The angular resolution in p_x-direction has been determined to be also 17 mrad (FWHM). By Gaussian error propagation of formula 5 (section 2.3.2) one can deduce the transversal momentum resolution which is hence also 17 mrad (FWHM). The same angular resolutions were also determined from the carbon tape measurements. Thus, by taking a conversion factor of 0.26 keV mrad^{-1} [35], the longitudinal momentum resolution, as given by the energy resolution of the HPGe-detector (see section 2.2.2), is about a factor 3.5 better compared to the transversal momentum resolution.

4.3. 4D-AMOC

In figure 7 the 4D-AMOC spectra of both samples are shown. The absolute value of the three-dimensional momentum of the electron annihilating with the positron as a function of the positron age is depicted. For each 4D-AMOC spectrum the count rate was about 0.3 s^{-1} and the total number of events was about 4×10^4. The number of positrons annihilating at the sample per second were about 6×10^5 [36].

4.3.1. Positron lifetime

By histogramming only the positron age of each event in the 4D-AMOC spectra we obtained two coincident positron lifetime spectra. In figure 8 the spectra as well as the fit of the positron lifetime components to the data are shown. Formula 1 from section 2.3.1 was used for the fit so that the absolute values of the residuals of the fit were as small as possible (figure 8).

Our instrument function $W(t)$ was determined from the gold foil measurement by fixing the positron lifetimes τ_1 and τ_2 to the values obtained by the PLEPS measurement (section 3). Additionally the ratio I_1/I_2 was kept constant as given by the measurements at PLEPS. With these boundary conditions we fitted through the positron lifetime spectrum of the gold foil. We received τ_3, I_1, I_2 and I_3 and the instrument function $W(t)$ consisting of two Gaussian distributions with an overall width of 540 ps (FWHM).

For the fitting procedure of the positron lifetimes and intensities of the carbon tape the above mentioned instrument function $W(t)$ from the gold foil measurement was used. Additionally τ_1, τ_2, τ_3 and I_1/I_2 were fixed as determined by the PLEPS measurements.

In table 1 the positron lifetimes and their respective intensities of the gold foil and the carbon tape are summarised for the measurements done at PLEPS and the SPM interface. The PLEPS values could be well reproduced at the 4D-AMOC measurements done at the SPM interface. The absolute values of the residuals of the fit of the positron lifetime spectra were for the gold foil and the carbon tape less than a value of about three (figure 8). τ_4 (carbon tape) of the measurement done at PLEPS could not be reproduced with the 4D-AMOC measurement. This can be explained on the one hand by the worse statistics at the SPM interface measurements as the positron lifetime spectra at PLEPS contained 100 times more events. On the other hand the peak to

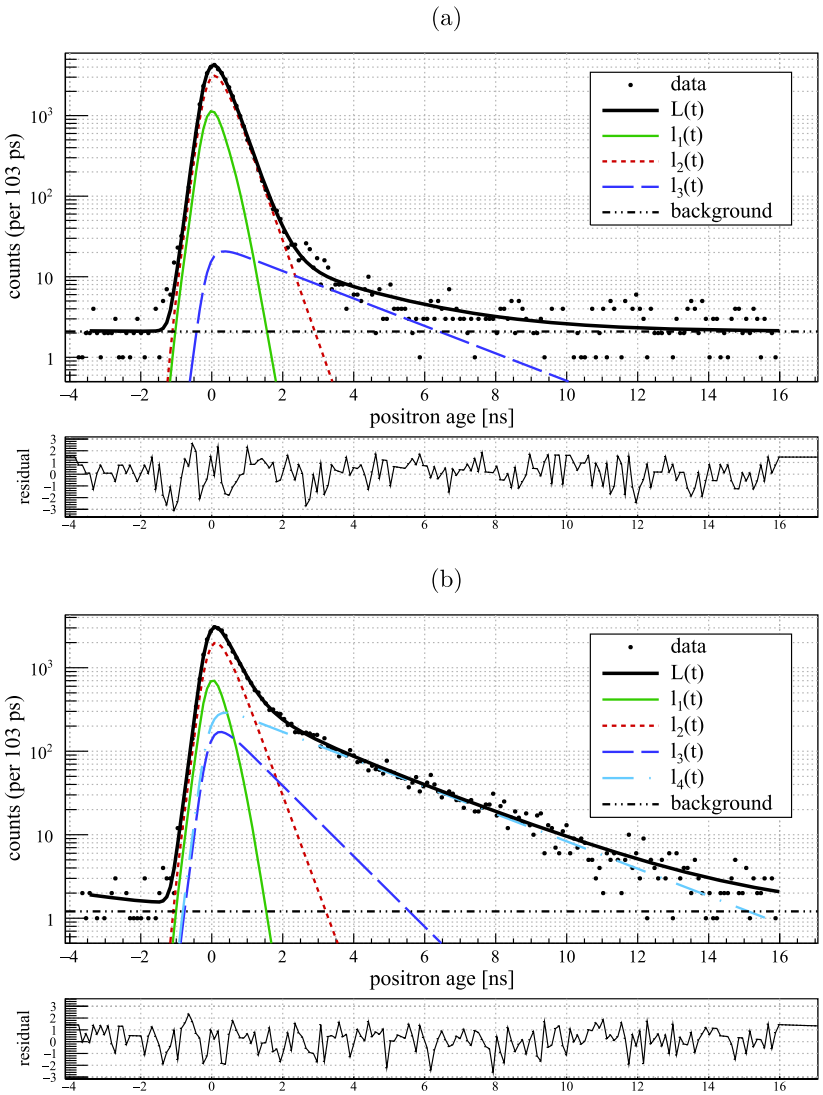

Figure 8. Positron lifetime spectra of (a) the gold foil and (b) the carbon tape. See table 1 for the obtained lifetimes and their intensities.

Table 1. Positron lifetimes and their intensities from the gold foil and the carbon tape measured at PLEPS (see section 3) and the SPM interface. Italic bold values were taken for the fit procedure of the positron lifetimes and intensities for the SPM interface measurements (for more details see text).

Gold foil	τ_1 (ps)	I_1(%)	τ_2 (ps)	I_2 (%)	τ_3 (ps)	I_3 (%)
PLEPS	***175***	***22.4***	***347***	***77.3***	2454	0.3
SPM intf.	175	22.1	347	76.1	2550	1.8

Carbon tape	τ_1 (ps)	I_1 (%)	τ_2 (ps)	I_2 (%)	τ_3 (ps)	I_3 (%)	τ_4 (ps)	I_4 (%)
PLEPS	***162***	***13.9***	***380***	***52.2***	***1029***	5.9	3013	28.0
SPM intf.	162	13.7	380	51.5	1029	7.8	2650	27.0

background ratio was a factor 100 better at the PLEPS measurements. Additionally the fact that not exactly the same piece of the carbon tape was taken for the measurements at PLEPS and at the SPM interface could have influenced the positron lifetime τ_4.

4.3.2. Annihilation probability

The measured positron lifetime spectra from figure 8 are given by the different possible states in which the positrons can annihilate. Equation (1) from section 2.3.1 can also be written as:

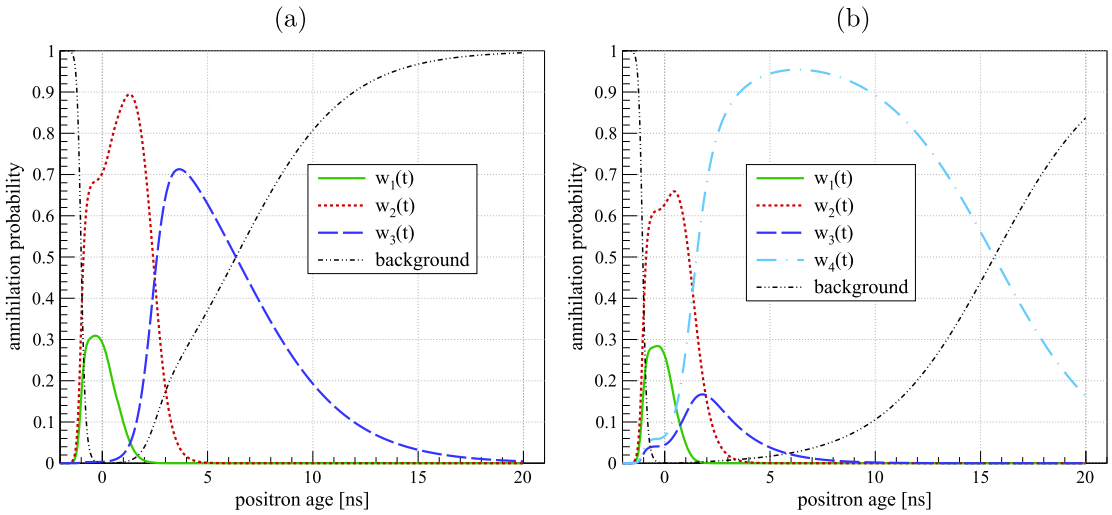

Figure 9. Time dependent annihilation probabilities of the positron states in (a) the gold foil and (b) the carbon tape.

$$L(t) = \sum_{i=1}^{N}\left[\frac{I_i}{\tau_i}\exp(-t/\tau_i) \ * \ W(t)\right] + \mathrm{BG}$$
$$= \sum_{i=1}^{N}\xi_i(t) + \mathrm{BG}. \tag{6}$$

The annihilation probability $w_i(t)$ or rather $w_b(t)$ that a positron is annihilating at the time t in the ith state or rather contributes to the background is given by:

$$w_i(t) = \frac{\xi_i(t)}{L(t)}, \quad w_b(t) = \frac{\mathrm{BG}}{L(t)}. \tag{7}$$

In figure 9 the positron age dependent annihilation probabilities from the gold foil and carbon tape measurements are depicted. For the calculation of the annihilation probabilities the positron lifetimes τ_i and intensities I_i were taken from figure 8 (table 1).

4.3.3. Absolute value of the three-dimensional electron momentum

By projecting the counts of the 4D-AMOC spectra from figure 7 onto the electron momentum axis we obtained the spectra of the absolute value of the three-dimensional electron momentum (figure 10(a)).

In figure 10(b) the ratio of the gold foil spectrum to the carbon tape spectrum is depicted. The ratio is smaller than 1 for momenta between $0 \times 10^{-3}\ m_0c$ and $15 \times 10^{-3}\ m_0c$ due to a more elevated valence electron contribution to the positron annihilation in the carbon tape (minimum ratio value: about 0.8). For momenta from $15 \times 10^{-3}\ m_0c$ to $40 \times 10^{-3}\ m_0c$ the ratio is larger than 1 (maximum ratio value: about 1.2) because of an increased core electron contribution of the gold foil. The statistical noise is larger than the mean ratios for momenta higher than $40 \times 10^{-3}\ m_0c$.

4.3.4. Momentum states

The mean absolute values of the three-dimensional electron momenta versus the positron age are plotted in figure 11. For each data point at least 1000 events were taken from the respective 4D-AMOC spectrum (figure 7).

The mean momenta of the gold foil (figure 11(a)) up to a value of 1.3 ns can be assigned to annihilation in vacancies and in surface states (see section 3). The maximum mean momentum value at about 3.9 ns is probably due to contaminants on the surface.

For the carbon tape (figure 11(b)) the mean momentum is at its lowest value at around 0 ns due to the contribution of para-positronium annihilation. The maximum at about 0.9 ns can be assigned to positrons that do not form positronium. Above circa 2 ns ortho-positronium annihilation gets dominant and contributes the most to the mean momentum. Up to a positron age of approximately 2.5 ns the shape of the mean momentum data of the carbon tape is comparable to 2D-AMOC data from e.g. [37] where the S parameter is plotted as a function of the positron age. (A high S parameter corresponds to a low mean momentum.) In our measurements the mean momentum rises again for positron ages above 2.5 ns while in [37] the S parameter stays constant. Due to the low statistics at higher positron ages this rise might not be significant.

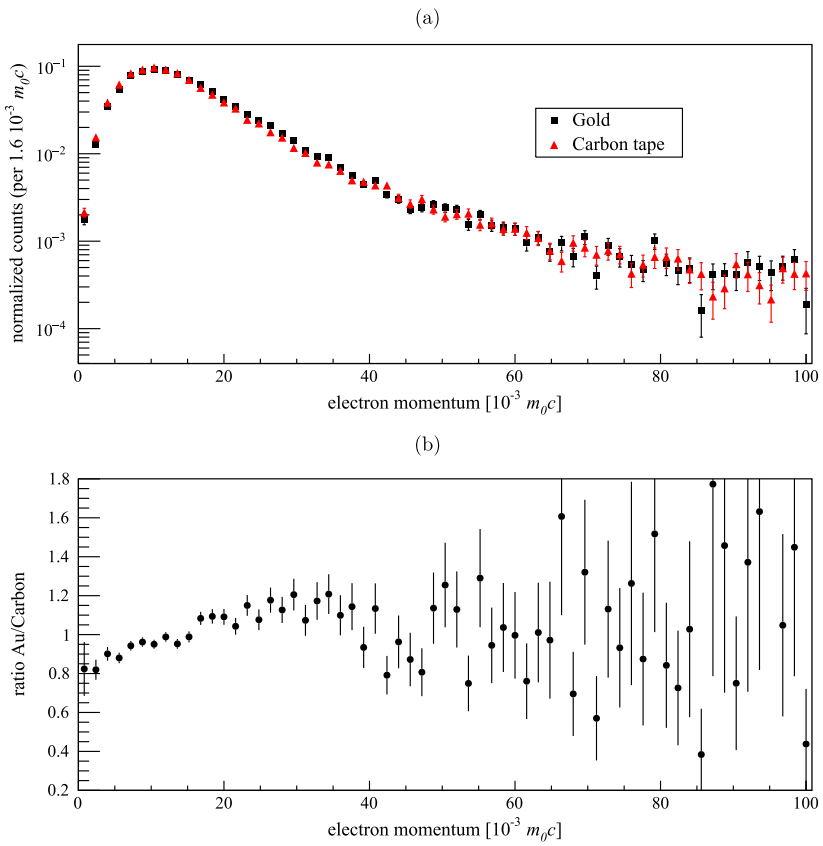

Figure 10. (a) Spectra of the absolute value of the three-dimensional electron momentum in gold ■ and carbon tape ▲. The integral of both spectra were normalised to 1. (b) Ratio Au/C of the top spectra.

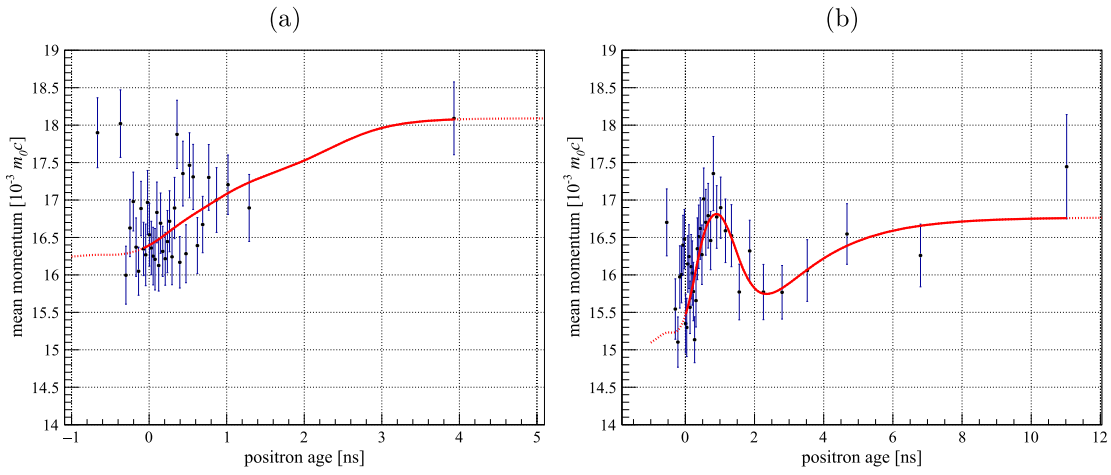

Figure 11. Mean absolute value of the three-dimensional electron momentum as a function of the time in the (a) gold foil and (b) carbon tape. The lines describe the fit through the data points (see formula 8). Only data points where the line is not dashed were taken into account for the fit.

By utilising the annihilation probabilities from figure 9 the discrete mean momentum states P_i could be derived by fitting the equation

$$P(t) = \sum_{i=1}^{N} P_i w_i(t) \tag{8}$$

to the data points from figure 11. To reduce the influence of the background (see figure 9), the fits were only performed in a range that is indicated by the solid lines. The sum over all w_i was normalised for each time thus one could write

Table 2. Discrete momentum states P_i derived from the gold foil and the carbon tape measurements. For each P_i the annihilation channel is specified.

	$P_1\,[10^{-3}\ m_0c]$	$P_2\,[10^{-3}\ m_0c]$	$P_3\,[10^{-3}\ m_0c]$	$P_4\,[10^{-3}\ m_0c]$
Gold foil	13.9 ± 1.0 Vacancies	17.3 ± 0.3 Surface states	18.1 ± 0.5 Contaminants on surf.	— —
Carbon tape	6.9 ± 1.5 Para-positronium	19.4 ± 0.6 Various defect sites	8.7 ± 2.2 Ortho-positronium	16.8 ± 0.3 Ortho-positronium

$$\sum_{i=1}^{N} w_i(t) = 1. \tag{9}$$

The discretized mean momentum states are summarised in table 2. These were not corrected for the three-dimensional momentum resolution of the 4D-AMOC setup. Due to their low annihilation probabilities (see figure 9), the states P_1 of the gold foil and P_1 and P_3 of the carbon tape have a higher confidence interval of the fit.

5. Summary and outlook

We have successfully performed first 4D-AMOC measurements at the SPM interface at the positron source NEPOMUC at the Munich research reactor FRM II. In 4D-AMOC measurements the three-dimensional electron momentum in coincidence with the positron age is determined. We used a position sensitive fast scintillation detector and a position sensitive HPGe-detector in coincidence to measure both annihilation quanta. The total time resolution of our setup was 540 ps (FWHM). We determined a transversal momentum resolution of about $17 \times 10^{-3}\ m_0c$ (FWHM) which was circa 3.5 times larger than the longitudinal momentum resolution.

Two samples (gold foil and carbon tape) were investigated at a positron implantation energy of 2 keV. We generated for each sample a 4D-AMOC spectrum where the absolute value of the three-dimensional electron momentum is depicted as a function of the positron age. From each 4D-AMOC spectrum a positron lifetime spectrum was derived and could be successfully verified with a lifetime measurement performed at PLEPS. Furthermore we deduced from the 4D-AMOC spectra discrete electron momentum states. The states of the carbon tape could be assigned to para-positronium and ortho-positronium annihilation. The momentum states which were dominant for the measurements with the gold foil can be related to annihilation in vacancies and surface states.

To establish 4D-AMOC in the future as a conventional positron annihilation method further improvements have to be made amongst others in count rate and momentum resolution. Thus, in order to fulfil the requirements, the active detector areas should be increased by an order of magnitude and the position resolution should be reduced to 1 mm (FWHM) or less which should be in principle possible [38, 39]. Additionally the sample-detector distance should be enhanced by a factor of about 2. A higher sensitivity of the detectors for the annihilation quanta as well as an elevated positron beam current (minimum factor 10) seem to be necessary to reveal the full potential of 4D-AMOC for defect characterisation. An improved total time resolution would be also helpful to obtain best defect characterisation possibilities.

Acknowledgments

We would like to thank Stephan Eschbaumer and Andreas Bergmaier for the support concerning the preparation of the sample chamber. Furthermore we would like to thank Christoph Hugenschmidt for providing us beam time at the positron source NEPOMUC. Fundings from the German BMBF (projects 05K10WNA-Posimethod and 05K13WN1-Posianalyse) and financial support by the Munich research reactor FRM II are gratefully acknowledged.

References

[1] Krause-Rehberg R and Leipner H S 1999 *Positron Annihilation in Semi-Conductors* ed M Cardona *et al* (Berlin: Springer)
[2] MacKenzie I K *et al* 1967 Temperature dependence of positron mean lives in metals *Phys. Rev. Lett.* **19** 946–8
[3] Berko S *et al* 1977 Momentum density measurements with a new multicounter two-dimensional angular correlation of annihilation radiation apparatus *Phys. Lett.* A **63** 335–8
[4] Lynn K G *et al* 1977 Positron-annihilation momentum profiles in aluminum: core contribution and the independent-particle model *Phys. Rev. Lett.* **38** 241–4

[5] MacDonald J R *et al* 1978 A two-dimensional doppler broadened technique in positron annihilation *Nucl. Instrum. Methods* **153** 189–94
[6] Sen P and MacKenzie I K 1977 Dual-parameter time and energy spectrometry in positron annihilation *Nucl. Instrum. Methods* **141** 293–8
[7] Reiner M *et al* 2014 *Ab-initio* calculation of CDB spectra—a case study on transition metals *J. Phys.: Conf. Ser.* **505** 012025
[8] Berko S 1983 Momentum density and fermi-surface measurements in metals by positron annihilation *Positrons in Solids Proc. Int. School of Physics 'Enrico Fermi'* vol 123 ed A Dupasquier and A P Mills Jr pp 64–145
[9] MacKenzie K 1983 Experimental methods of annihilation time and energy spectrometry *Positrons in Solids Proc. Int. School of Physics 'Enrico Fermi'* vol 123 ed A Dupasquier and A P Mills Jr pp 196–264
[10] Hautojärvi P and Corbel C 1995 Positron spectroscopy of defects in metals and semiconductors *Positron Spectroscopy of Solids Proc. Int. School of Physics 'Enrico Fermi'* vol 125 ed A Dupasquier and A P Mills Jr (Amsterdam: IOS Press) pp 491–532
[11] Mitteneder J *et al* 2016 Micrometer positron beam characterization at the scanning positron microscope interface *J. Phys.: Conf. Ser.* accepted
[12] Piochacz C *et al* 2007 Implementation of the munich scanning positron microscope at the positron source nepomuc *Phys. Status Solidi* c **4** 4028–31
[13] Piochacz C 2009 Generation of a high-brightness pulsed positron beam for the Munich scanning positron microscope *PhD Thesis* Technische Universität München (http://nbn-resolving.de/urn/resolver.pl?urn:nbn:de:bvb:91-diss-20091123-829689-1-1)
[14] Hugenschmidt C 2010 Positron sources and positron beams *Physics with Many Positrons Proc. Int. School of Physics Enrico Fermi* vol 174 ed A Dupasquier and A P Mills Jr pp 399–417
[15] Hugenschmidt C *et al* 2014 Positron beam characteristics at NEPOMUC upgrade *J. Phys.: Conf. Ser.* **505** 012029
[16] Löwe B *et al* 2013 A position sensitive germanium detector for the measurement of angular deviation of annihilation radiation *J. Phys.: Conf. Ser.* **443** 012098
[17] Ackermann U *et al* 2016 Position and time resolution measurements with a microchannel plate image intensifier: a comparison of monolithic and pixelated $CeBr_3$ scintillators *Nuclear Instrum. Meth. Phys. Res.* A **823** 56– 64
[18] Schödlbauer D *et al* 1988 A pulsing system for low energy positrons *Nuclear Instrum. Meth. Phys. Res.* B **34** 258–68
[19] Sperr P *et al* 1997 Pulsing of low energy positron beams *Appl. Surf. Sci.* **116** 78–81
[20] ROOT. CERN https://root.cern.ch/
[21] Brun R and Rademakers F 1997 ROOT—an object oriented data analysis framework *Nuclear Instrum. Meth. Phys. Res.* A **389** 81–6
[22] Qt.Version 5.2.1. The Qt Company https://qt.io
[23] Schaile O 2005 Histpresent—easy interactive analysis within the ROOT framework *ROOT2005 WORKSHOP* (http://bl.physik.uni-muenchen.de/marabou/htmldoc/hpr.pdf)
[24] Marabou http://bl.physik.uni-muenchen.de/marabou/htmldoc
[25] Lutter R *et al* 1999 Marabou—a mbs and root based online/offline utility *Santa Fe 1999: 11th IEEE NPSS Real Time Conf. 1999* pp 363–6
[26] *Electron Microscopy Sciences Conductive Adhesives Tabs, Tapes, and Sheets* (https://emsdiasum.com/microscopy/products/sem/conductive.aspx)
[27] Egger W 2010 Pulsed low-energy positron beams in materials sciences *Physics with many Positrons Proc. Int. School of Physics 'Enrico Fermi'* vol 174 ed R Brusa (Amsterdam: IOS Press) pp 419–49
[28] Sperr P *et al* 2008 Status of the pulsed low energy positron beam system (PLEPS) at the munich research reactor FRM-II *Appl. Surf. Sci.* **255** 35–8
[29] Corbel C *et al* 1983 Computed positron lifetimes in vacancies and vacancy-iron clusters in gold *Radiat. Eff.* **79** 305–12
[30] Corbel C 1986 Temps de vie du positon dans des amas lacunaires application a l'étude de l'interaction lacunes-impuretés *PhD Thesis* Centre d'Études Nucléaires de Fontenay-aux-Roses (www.iaea.org/inis/collection/NCLCollectionStore/_Public/17/058/17058591.pdf)
[31] Nieminen R M and Hodges C H 1978 Plasmon model for image-potential-induced surface states with an application to positrons at metal surfaces *Phys. Rev.* B **18** 2568–76
[32] Jean Y C 1990 Positron annihilation spectroscopy for chemical analysis: a novel probe for microstructural analysis of polymers *Microchem. J.* **42** 72–102
[33] Egger W *et al* 2008 Investigations of epoxy-based adhesives with PLEPS *Appl. Surf. Sci.* **255** 209–12
[34] West R N 1995 Positron studies of the electronic structure of solids *Positron Spectroscopy of Solids Proc. Int. School of Physics 'Enrico Fermi'* vol 125 ed A Dupasquier and A P Mills Jr (Amsterdam: IOS Press) pp 75–143
[35] Mogensen O E 1995 *Positron Annihilation in Chemistry* ed F Schäfer *et al* (Berlin: Springer) (doi:10.1007/978-3-642-85123-0)
[36] Dickmann M *et al* 2016 Radio frequency elevator for a pulsed positron beam *Nuclear Instrum. Meth. Phys. Res.* A **821** 40–3
[37] Sato K *et al* 2009 Probing the elemental environment around the free volume in polymers with positron annihilation age-momentum correlation spectroscopy *Macromolecules* **42** 4853–7
[38] Johnson L C *et al* 2011 Characterization of a high-purity germanium detector for small-animal SPECT *Phys. Med. Biol.* **56** 5877–88
[39] Seifert S *et al* 2013 First characterization of a digital SiPM based time-of-flight PET detector with 1 mm spatial resolution *Phys. Med. Biol.* **58** 3061–74